Dendrite growth in BME and PME ceramic capacitors

Jaemi Herzberger*, Alexander Teverovsky**

*NASA Space Technology Research Fellowship Student, University of Maryland
**Dell Services Federal Government, Inc.
NASA/GSFC, code 562, Greenbelt, MD 20771
Alexander.A.Teverovsky@nasa.gov

I. Introduction

Multilayer ceramic capacitors (MLCCs) constitute the majority of components used in electronic assemblies, and most of their failures are related to cracks that are caused either by insufficient process control during manufacturing, by thermal shock associated with soldering, or by flex cracking during handling and/or mechanical testing of the circuit boards. The failure mode varies from excessive leakage currents or a short circuit to intermittent or "noisy" behavior that in some cases might be misjudged as software failures. The intermittent failures are extremely difficult to detect, so electrochemical migration in cracks is indeed the reason of failures that have been labeled: ''no failures found'' [1].

Historically, first ceramic capacitors were manufactured with silver, and later with silver/palladium electrodes, so-called precious metal electrode (PME) capacitors, and the low-voltage failure phenomenon in these parts was attributed to silver [2-3] or palladium [4] migration in cracks that results in dendrite growth and intermittent short circuits in capacitors. Although both metals, Ag and Pd, can form dendrites, silver is considered a metal that is the most susceptible to electrochemical migration (ECM) compared to other metals because it does not passivate, is very soluble anodically, and its hydroxides also have good solubility [5]. Silver migration was observed at voltages as low as 0.4 V [6] and relative humidity ~ 40% relative humidity (RH) [7].

It is known that addition of more than 10% Pd reduces ECM of the Ag/Pd alloys substantially [6], and according to Lin and Chan [8] dendrite growth ceases completely at 30% Pd. The effect was ascribed to formation of PdO, which is derived either from firing at 400-700 °C or from anodic polarization, that passivates the electrode surface, and blocks dissolution of silver. However, silver migration still can happen in MLCCs with Ag/Pd electrodes, and one of the possible mechanisms is related to diffusion of silver into barium-titanate ceramic during high-temperature sintering [9]. This diffusion facilitates silver migration and dendrite growth along the grain boundaries of ceramics, thus making the supply of Ag from electrodes less critical.

It is generally assumed that there are three processes involved in the formation of dendrites: (i) anodic dissolution, (ii) transportation of metallic ions, and (iii) dendrite growth. In many cases, the first one, generation of ions, plays the most important role. Yang and Christou [10] studied ECM of silver in test structures consisting of conductive elastomer land grid array sockets and found that the formation of dendrites is not the primary cause of leakage current degradation. Instead, the failure occurs when surface insulation resistance drops substantially, due to silver ion accumulation, to a critical concentration prior to the dendritic formation.

A specific feature of low-voltage failures (LVFs) is that the short circuit formed at low voltages by a dendrite clears as soon as high voltage is applied, due to the blown-fuse effect. For this reason, humidity steady-state low voltage (HSSLV) lot acceptance testing per MIL-PRF-123 (240 hours at 85°C, 85% RH) is carried out at 1.3 V, and the post-test insulation resistance (IR) is also measured at 1.3 V. In addition, to further preserve the short circuit condition, the testing and IR measurements should be carried out using 100 kOhm resistors connected in series to the capacitors under test.

Investigation of the suitability of HSSLV testing for military-grade ceramic capacitors by the NASA Engineering and Safety Center (NESC) showed [11] that for the last 10 years there has been a low incidence rate of field failures for high and established reliability PME MLCCs in low voltage circuit applications. Although historically LVFs were attributed to lots with large proportions of manufacturing defects, currently, these failures are more likely to be caused by cracking due to soldering and handling of the parts. It was concluded that the HSSLV testing is not a value-added test and is not necessary for lot acceptance of MLCCs manufactured per military specifications by the

qualified product list (QPL) manufacturers. However, the effectiveness of HSSLV testing for commercial base-metal-electrode (BME) capacitors has not been evaluated.

Electrochemical migration and dendrite growth of Ni has not been studied in detail yet, and the available data are controversial. One of the first studies of ECM capability of different metals commonly used in the electronics industry has been performed by DerMarderosian in 1978 [12]. Using a water drop test (WDT), he showed that Ag, Cu, Sn, Cd, Bi, Zn, and Pb form dendrites in distilled water, while Au, Pd and In were found to migrate only after the addition of halogen compounds, such as KCl or NaCl. Metals such as Cr, Fe, and Ni might migrate in some special conditions only. Analysis of ECM of different metals shows that silver and copper can migrate under humid conditions in an adsorbed water layer, while other susceptible metals such as Sn, Ni, Pb, Pd, etc. require a visible water layer (condensed conditions) [1]. In general, most metals used in electronic assemblies are susceptible to migration, and only metals that cannot be electroplated (such as aluminum) from aqueous solutions can be regarded as safe from ECM.

According to DiGiacomo [13], Ni dendritic growths had the highest voltage threshold experienced in WDT: Ni fails to migrate at an applied potential of 1.6 V and lower, while for Ag the minimum potential is a fraction of a volt and for Cu it varies below 1 V, depending on the state of oxidation. Ni migration is also greatly reduced with the growth of oxide or hydroxide films. Noh [14] investigated ECM in flexible PWBs during water drop testing. The growth rate of dendrites from the cathode to the anode decreased with the following order of surface finish material: Cu, electroless Ni, and electroless nickel-immersion gold.

Zheng et al. [15] studied leakage current degradation in piezoelectric samples of lead zirconate titanate (PZT) ceramic with Ni electrodes in humid environments. At relatively high voltages (240 V) and humidity (90% RH), a significant fluctuation of the leakage currents was observed. Degradation of the leakage currents with time featured transients that were explained by the electromigration/breakdown mechanism, according to which nickel filaments grow in the conductive channels from the cathode to anode and a local breakdown, which burns them out when the filament comes close enough to the anode, resulting in a current transient.

A review of the literature data on Ni migration indicates that Ni was considered to be a non-migrating metal in some studies, but has been found to grow dendrites in others. Harsani [16] carried out WDT on samples with Ni electrodes and showed an anomalous behavior: contrary to samples with Ag and Cu that follow a classical dendrite growth model, Ni dendrites were formed on the anode. The process was attributed to the formation of $HNiO_2^-$ cations and deposition of Ni_3O_4 at the anode.

Based on literature data, one might expect different electrochemical processes and mechanisms of IR degradation for BME and PME capacitors during low-voltage testing in humid environments. In this work, water layer testing was developed to mimic processes in cracks and was used for in-situ, high-power, optical observations of electrochemical migration and dendrite growth in BME and PME capacitors. To compare ECM processes on wet surfaces and surfaces with adsorbed moisture, cross-sectioned capacitors were tested using HSSLV testing. Scanning electron microscopy (SEM) and energy dispersive spectroscopy (EDS) were used to study materials and morphology of the dendrites and deposits. Specifics of failure mechanisms in BME and PME capacitors are discussed.

II. Experiment

Four PME and five BME types of large size (from 1812 to 2225) X7R capacitors produced by different vendors were used in this study. Most PME capacitors were manufactured to military specifications and all BME capacitors were built to commercial specifications. The capacitance varied from 0.1 μF to 1 μF and the rated voltage (VR) was 50 V or 100 V. The specific features of the parts used, including the thickness of the dielectric layers, number of electrodes, and materials of the terminals are shown in Table 1. The type of solder used is shown in parenthesis.

To expose internal electrodes to the environmental conditions and simulate electrochemical processes in capacitors with cracks, the parts were perpendicularly cross-sectioned to the internal electrodes. Before cross-sectioning, thin wires were soldered to the terminals using an eutectic Sn/Pb solder. Then, the parts were molded with epoxy, ground and polished on the side opposite to the leads, and thoroughly rinsed with deionized water and isopropanol. Two types of testing were used for cross-sectioned parts: water layer testing (WLT) and standard HSSLV testing.

Table 1. Characteristics of capacitors.

Part	Type	Mfr.	Size	Dielectric thickness, um	Number of electrodes	Termination: base metal, barrier, finish (solder)
0.1µF, 100V	PME	P	1825	52.5	18	Ag-Ni-Sn (Sn60/Pb40)
1µF, 50V	PME	A	2220	29	38	Ag-Ni-Sn (Sn60/Pb40)
0.47µF, 50V	PME	C	1825	22	28	Ag-Ni-Sn70/Pb30 *
0.47µF, 50V	PME	V	1825	21.5	26	Cu-Ni-Sn *
0.47µF, 50V	BME	C	1825	21	24	Cu-Ni-Sn *
0.47µF, 50V	BME	A	1825	28	26	Cu-Ni-Sn *
1µF, 50V	BME	M	2220	19	44	Cu-Ni-Sn (Sn60/Pb40)
1µF, 50V	BME	C	2225	14	26	Cu-Ni-Sn (Sn60/Pb40)
1µF, 50V	BME	C	1812	12	50	Cu-Ni-Sn (Sn60/Pb40)

*the same eutectic solder was used for these parts, but to minimize its effect, solder was applied only to the corners of the parts that are opposite to the cross-sectioned surface.

The WLT technique is similar to the well known water drop testing, but limits the thickness of the water layer to a few micrometers, thus making test conditions closer to the conditions in cracks with condensed water. To avoid the effects from contamination, distilled water and a quartz 1 mm optical plate were used. Currents during the testing were monitored using a data logger, and the development of dendrites was observed and recorded with time using a high-power inverted metallurgical microscope. The test set-up that allowed in-situ observation of dendrite growth in cross-sectioned samples is shown in Figure II.1.

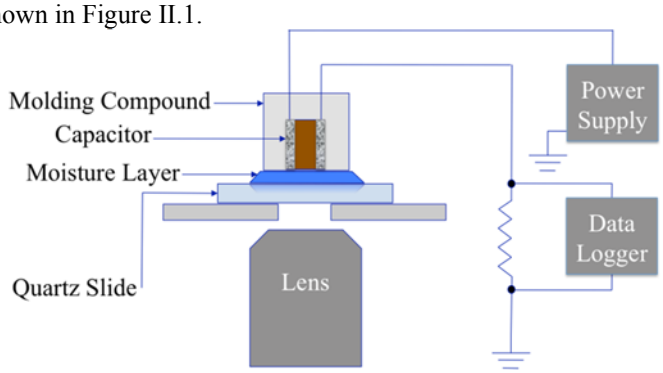

Figure II.1. Schematic of the water layer test set-up.

Standard HSSLV testing at 85°C, 85% RH, 1.3 V, 240 hours was used to simulate conditions when only a few monolayers of water (from 2 to 6 based on literature data) are absorbed on the surface of cracks, or condensed in fine cracks of a thickness in the nanometer range. In this case, the bias was applied through 10 kOhm or 100 kOhm resistors, and the currents were monitored using a data logger.

III. Water layer test results

Typical variations of leakage currents in cross-sectioned BME and PME capacitors during WLT are shown in Figure III.1. The test conditions varied by voltage, from 0.5 V to 1.3 V, and the thickness of the water layer, from ~3 µm to ~ 35 µm. In most cases, the initial level of leakage current was in the range from 3×10^{-8} to 5×10^{-7} A, and sharply increased to more than 10^{-5} A (due to 100 kOhm limiting resistors) after some time of testing, indicating a short circuit failure. Variations in voltage almost exponentially increased leakage currents, whereas an increase in the moisture layer thickness raised currents to a much lesser degree, almost linearly. Depending on test conditions, the time to failure (TTF) varied from a few minutes to a few hours. TTF did not change substantially at voltages between 0.8 V and 1.3 V, but tended to increase at 0.5 V.

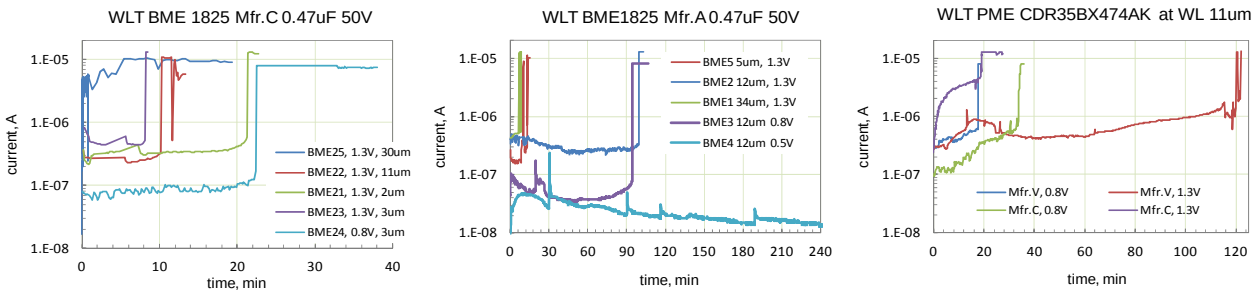

Figure III.1. Variations of currents with time during water layer testing at different conditions for BME (a, b) and PME (c) capacitors.

In some cases, after a failure the currents dropped and then increased again indicating a "classical" intermittent behavior. Optical observations showed that in all cases the short circuit conditions corresponded to dendrites bridging electrodes and terminal metallization. The recovery of currents occurred after the dendrite rupture, as illustrated in Figure III.2.

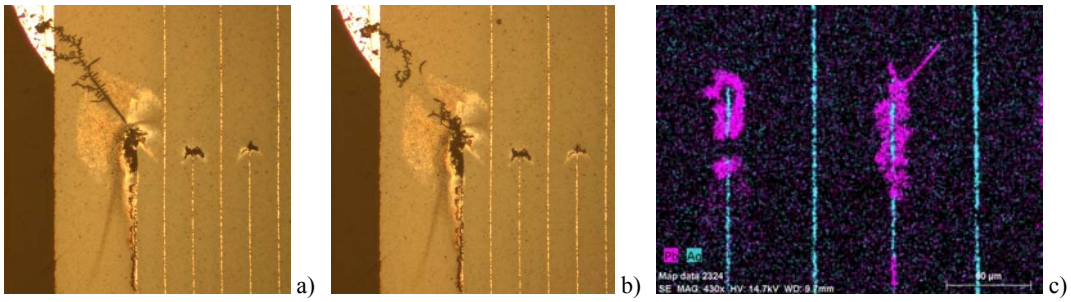

Figure III.2. Lead-rich dendrite on the surface of 1825, 0.1 µF, 100 V, Mfr.P, PME capacitor that shorted after 3.6 min at 1.3V before (a) and after (b) dendrite rupture. Figure (c) shows EDS mapping of similar dendrites from a different site.

EDS analysis of the dendrites showed that contrary to expectations, the dendrites were composed not of silver, but of lead. Note that a eutectic Sn/Pb solder was used to solder wires to the terminals in this part. Additional tests showed that lead-rich dendrites were growing at voltages as low as 0.5 V (see Figure III.3). Similar to the previous case, the shorting dendrites grew from the tip of the cathode electrode, closest to the edges of the anode terminal. The following EDS analysis indicated lead deposits and dendrites at the tips of other cathode electrodes as well.

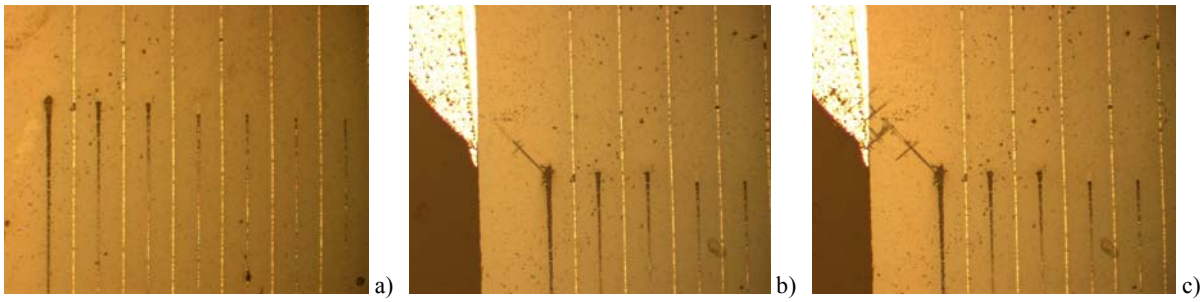

Figure III.3. Formation of dendrites at the tips of Ag/Pd electrodes on 1825 0.1 µF 100V Mfr. P PME capacitor at 0.5 V 100 min (a), 0.8 V 5min (b), and 0.8 V 12 min (c).

Analysis of 2220 1 µF 50 V BME capacitors after WLT at 1.3 V, with terminals soldered using a Sn/Pb alloy, also revealed the formation of lead dendrites at the tips of the cathode electrodes, as shown in Figure III.4. Lead-containing deposits were formed also on the surface of the end margin area, close to the anode terminal.

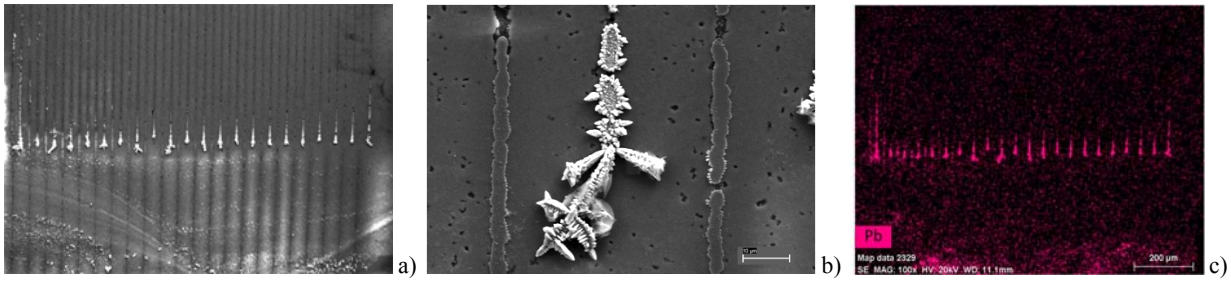

Figure III.4. Overall (a) and close-up (b) SEM views of dendrites that formed on the surface of a 2220 BME 1.0 µF 50 V Mfr. M capacitor after 40 mins at 1.3V. Figure (c) shows an EDS mapping of the area shown in Figure (a). Note that EDS analysis also indicated the presence of carbon in the lead-rich areas.

Analysis of another 2220 BME 1.0 µF 50V capacitor, that failed after 100 minutes of WLT at 1.3V, (see Figures III.5, 6) showed the presence of both tin and lead in the composition of the dendrites. Some areas of the Sn/Pb solder surrounding the anode terminal were corroded, and had large SnO crystals occurring on the surface. Small SnO crystals were observed on the end margin surface of the capacitor, between the terminal and tips of the cathode electrodes.

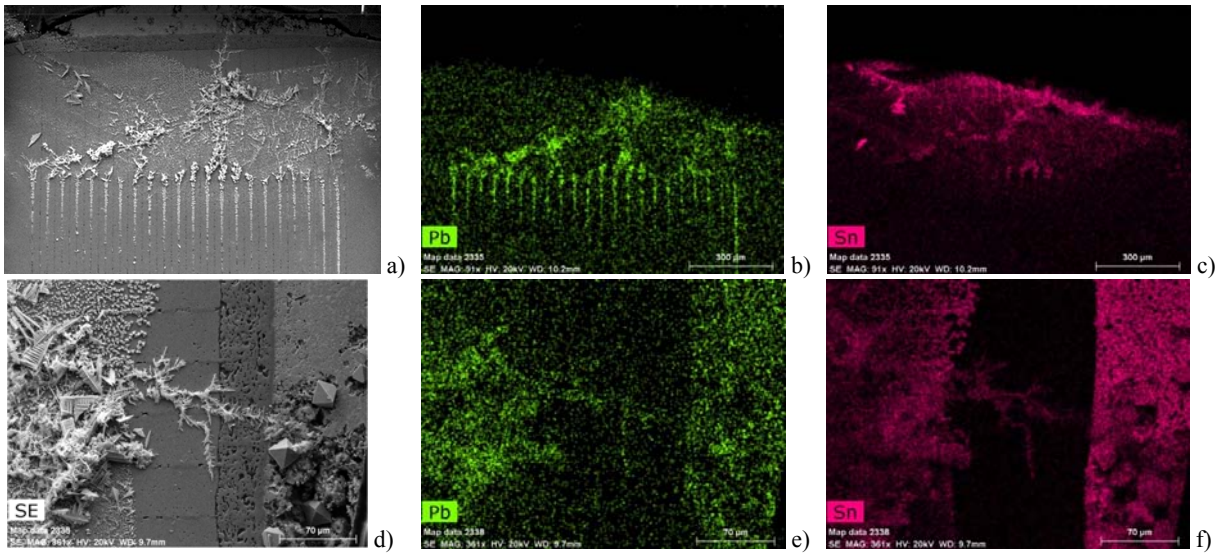

Figure III.5. Overall SEM view (a) and Pb (b) and Sn (c) EDS mapping of the 2220 BME 1.0 µF 50 V capacitor after 100 mins of 1.3 V WLT. Figures d, e, and f show close-ups of the dendrite and the relevant EDS maps.

Two types of dendrites were observed: tin-rich and lead-rich. Lead-rich dendrites appeared to form needle-like structures, whereas tin-rich dendrites formed fern-like structures (see Figure III.6).

Testing of a 2220 BME 1.0 µF 50 V capacitor at 0.5 V for 24 hours did not result in a short circuit failure; however, optical and SEM analysis revealed deposits of Sn and Pb along the cathode electrodes, as shown in Figure III.7. Layers of tin-containing and lead-containing deposits (with some carbon presence) are clearly seen on the surface of the anode end margin area, parallel to the cathode tips.

Copper deposits were observed on another sample of these parts tested at 0.25 V for 96 hours. Again, no electrical failure occurred, but the presence of deposits was detected during SEM/EDS examinations of the part (see Figure III.8).

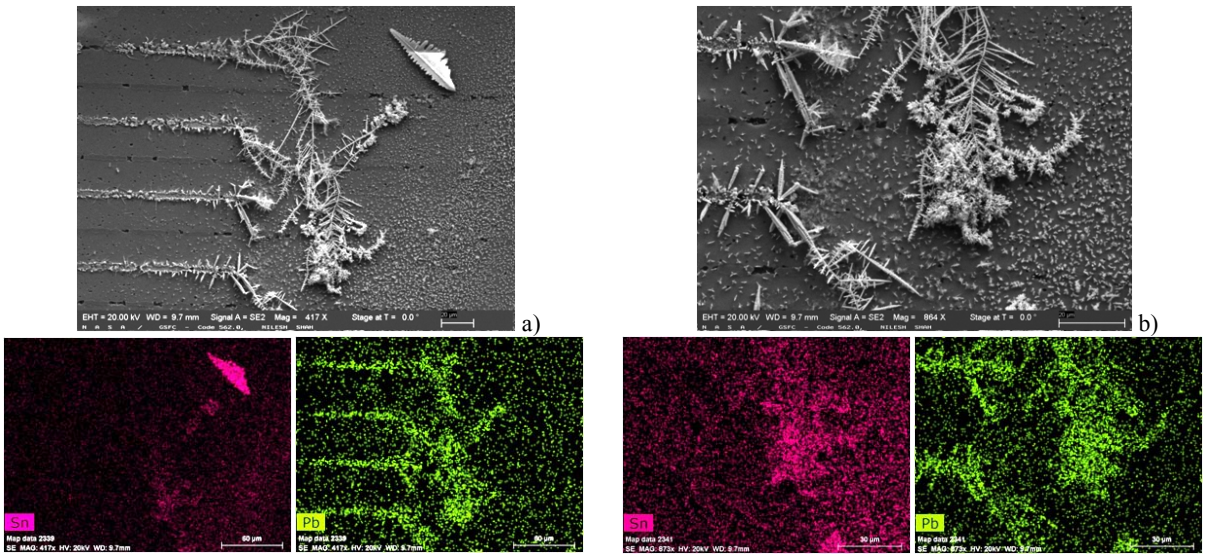

Figure III.6. Examples of tin-rich and lead-rich dendrites on the sample shown in Figure III.5. A fern-like leaf in the top right corner of figure (a) is a piece of tin dendrite that broke-off from the stem and was displaced in SEM.

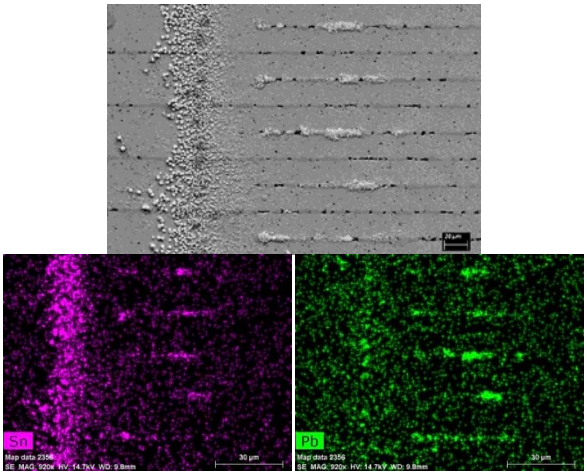

Figure III.7. SEM view and EDS mapping of the 2220 BME 1.0 µF 50 V Mfr. M capacitor (MLCC4) at 0.5 V after 24 hours (no short).

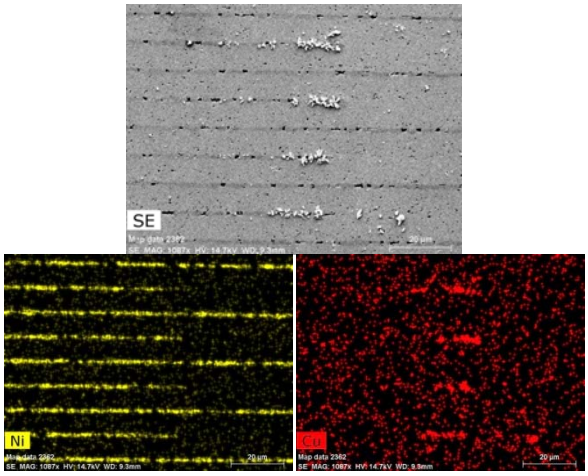

Figure III.8. Copper deposits at the tips of cathode electrodes on 2220 BME 1.0 µF 50 V Mfr. M capacitor (MLCC5) after 17 hours WLT at 0.25V (no short after 96 hr)

WLT of PME capacitors with a pure tin finish resulted in the formation of tin containing deposits along the tips of the cathode electrodes. Some tin dendrites were growing not from cathodes, but from the tin-containing deposits (see Figure III.9).

Similar to the pure tin finish on PME capacitors, WLT of PME capacitors with Sn/Pb finish, tested at 0.8 V, resulted in the halo formation of deposits around the cathode tips and dendrite growth at the periphery, that resulted eventually in a short circuit failure. However, contrary to the previous case, the deposits and dendrites consisted of tin-rich and lead-rich compositions. Examples of such deposits are shown in Figure III.10. Figure III.11 clearly shows that the tin-rich and lead-rich dendrites grow not from the silver cathodes, but from the tin and lead depositions formed around the edge cathodes.

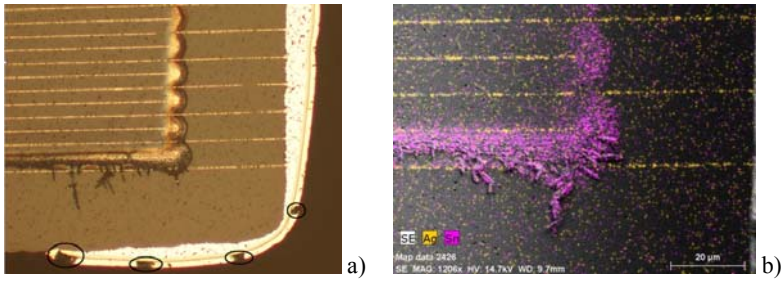

Figure III.9. Optical (a) and SEM/EDS map (b) images of a PME 0.47 µF 50 V Mfr. V capacitor shorted after 18 min at 0.8 V of WLT. Marks on Figure (a) indicate locations of tin termination corrosion.

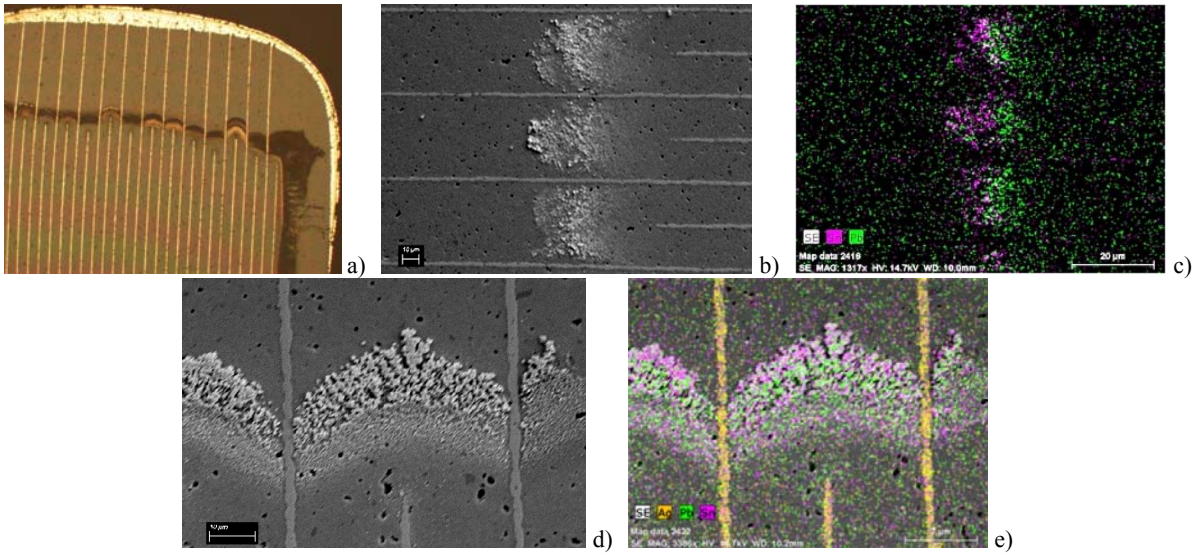

Figure III.10. Optical (a), SEM (b) and EDS (c) mapping images of a 0.47 µF 50 V PME capacitor from Mfr. C (Sn/Pb finish) that failed due to a short circuit after 35 minutes at 0.8 V during WLT. Figures (d) and (e) show another area of the tin and lead deposits. Note that in all cases, tin and lead are at somewhat different locations.

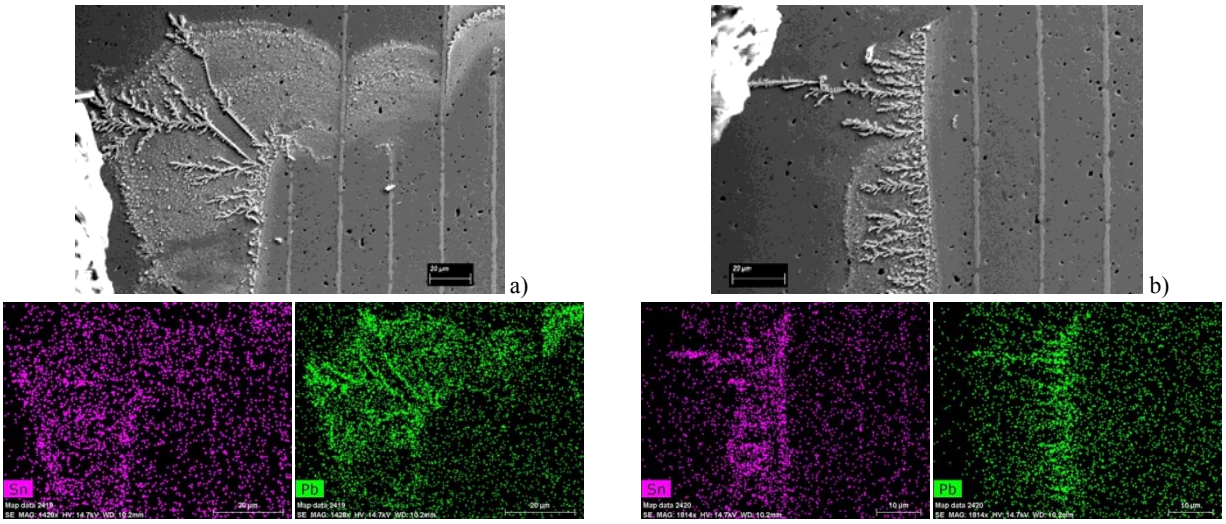

Figure III.11. Tin and lead deposits and dendrites growing from deposits near the edge electrodes of a 0.47 µF 50 V PME capacitor from Mfr. C that failed during WLT at 0.8 V in 35 minutes.

Testing of an 1825 PME 0.47 µF 50 V capacitor at 0.5 V for 2.5 hours resulted in a short circuit failure. Optical and SEM analysis revealed the formation of a long tin dendrite that bridged the tip of the cathode electrode and the anode terminal. Note that the solder was minimized on this capacitor and applied only on the opposite corner from the cross-sectioned surface, so the finish remained pure tin. The depletion of the tin finish layer, along with the particular pathway of the dendrite toward the depleted area observed for this part, is an indicator that dissolved Sn^{+} ions formed this dendrite.

Testing of BME capacitors that had a pure tin finish metallization revealed copper and tin dendrites growing at 1.3 V and 0.8 V. Figure III.12 shows an example of a copper dendrite that caused the failure of a 0.47 µF 50 V Mfr. C 1825 capacitor at 1.3V after 5.4 hours. Note the extensive pitting corrosion of the copper base metallization that obviously provided Cu^{2+} ions for the dendrite growth.

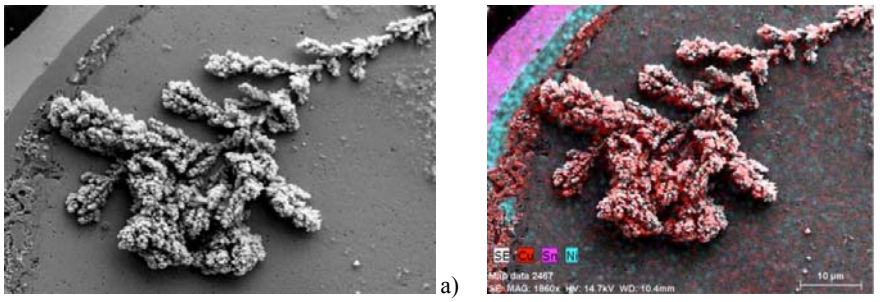

Figure III.12. SEM (a) and EDS mapping (b) images of an 1825 BME 0.47 µF 50 V Mfr. C capacitor that failed after 5.4 hours at 1.3V. Note that the copper dendrite was displaced during SEM examinations.

Figure III.13 shows a 0.47 µF 50 V 1825 capacitor from Mfr. A that failed during WLT after 1.4 hours at 1.3 V. Figure III.14 presents close-up images of dendrites shown in the last cathode electrode at the right side of Figure III.13.b. Both, copper and tin deposits and dendrites were formed at the cathode tips; however, copper tends to form deposits first, and closer to the nickel electrodes. With time, the migration of tin begins, halting the migration of copper, and eventually tin dendrites result in the short circuit failure. Tin-containing deposits formed several layers of halo arrangements on the end margin area around the cathode tips.

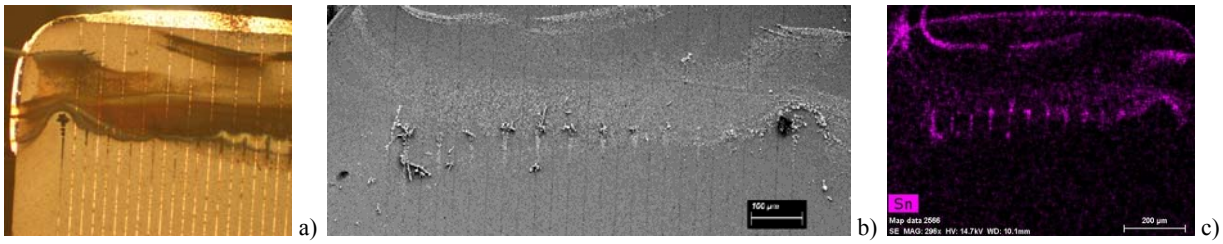

Figure III.13. Optical (a), overall SEM (b), and EDS mapping of Sn deposits and dendrites (c) in a 0.47 µF 50 V 1825 capacitor, Mfr. A, that failed during WLT after 1.4 hour at 1.3 V. Note that some dendrites were displaced during SEM examinations.

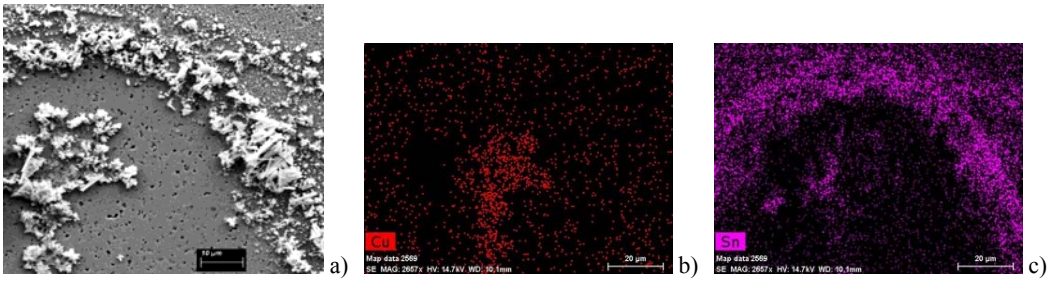

Figure III.14. A close-up SEM view (a) and EDS mapping of deposits shown at the right cathode electrode in Figure III.13.b.

Analysis of the kinetics of dendrite growth on the 1825 BME 0.47 µF 50 V Mfr. A capacitor at 1.3V shows that the copper base terminal metallization initially darkens, which spurs the growth of copper dendrites from the edge cathode electrode. This process continues for ~6 min, after which the tin finish area starts depleting, indicating the dissolution and electrochemical migration of the tin. This development is concurrent with long dendrite formations that quickly begin extending from the copper dendrites. SEM and EDS analysis showed that these long formations

were tin. The part failed after 8 min of testing, when the long tin formations branched back to the tin finish on the terminal. Figure III.15 shows optical images, and Figure III.16 shows SEM and EDS mapping images of the dendrite formations.

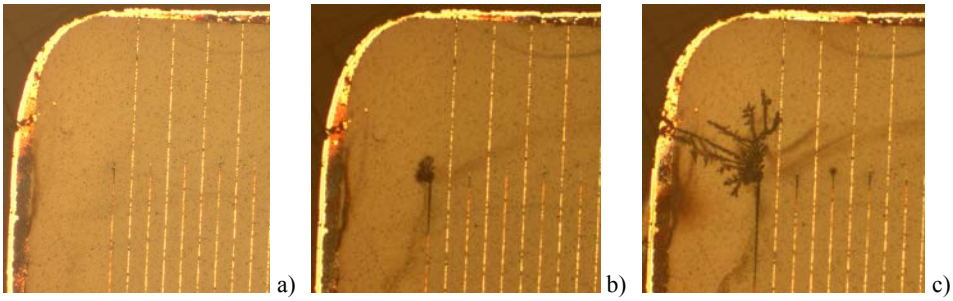

Figure III.15. Optical images of an 1825 BME 0.47 µF 50 V, Mfr. A capacitor after 3 min (a), 6 min (b), and 8 min (c) of water layer testing at 1.3 V. Note the areas of darkening Cu metal base layer at the termination in all three pictures that indicate pitting corrosion of Cu. Depletion of the tin finish area across the dendrite in figure (c) indicates the anodic dissolution of tin.

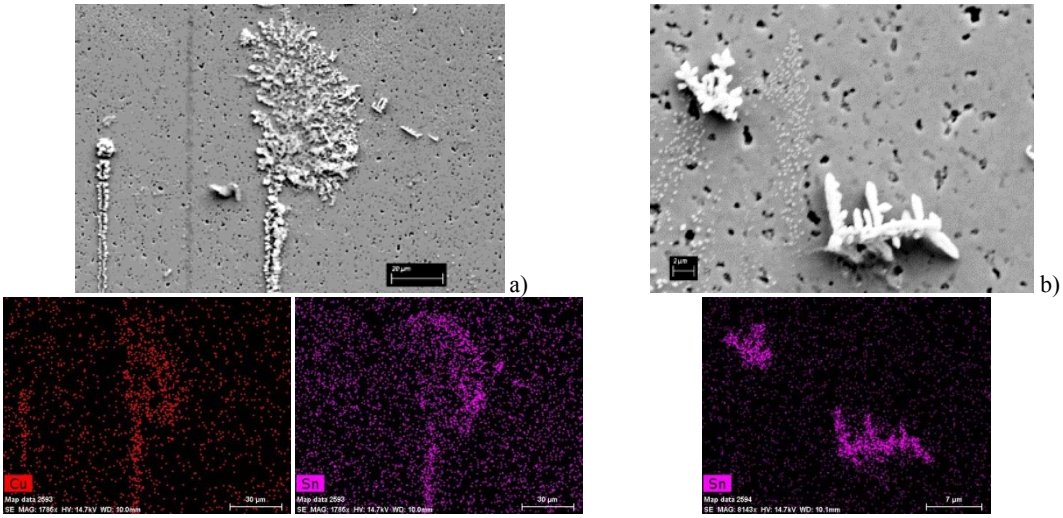

Figure III.16. SEM images and EDS mapping of the dendrites shown in Figure III.15 (c). Note that the long tin dendrites broke off from the Cu/Sn dendrites shown in figure (a) and were displaced during SEM examinations. Figure (b) shows remnants of the Sn dendrites.

Testing of an 1825 BME 0.47 µF 50 V capacitor from Mfr. C at 0.8 V resulted in a short circuit failure after 23 minutes of testing. Analysis showed that the failure was due to a tin dendrite growth as shown in Figure III.17. Severe corrosion at the bottom edge of the tin finish metallization indicates the area that provided tin ions for the dendrites growth.

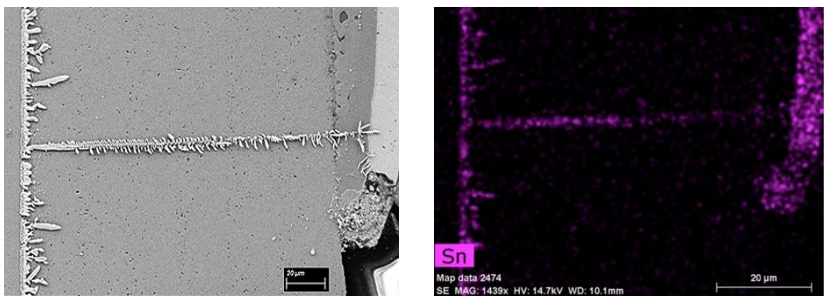

Figure III.17. Tin dendrite growth at the edge cathode electrode in a BME 1825 0.47 µF 50 V capacitor from Mfr. C that failed at 0.8 V after 23 minutes of testing.

The results of WLT for the 1825 0.47 µF 50 V BME capacitors from Mfr. A at 0.8 V and 0.5 V are shown in Figures III.18 and III.19. In both cases, the thickness of the water layer was ~ 12 um. At 0.8 V, the part failed after ~ 1.5 hours of the testing, and at 0.5 V, no failures occur even after 4 hours. However, testing of another 1825 PME 0.47 µF 50 V capacitor at 0.5 V for 2.5 hours did result in tin dendrite growth that caused a short circuit failure. Tin dendrite growth at the tip of the end cathode electrode at 0.8 V occurred along the pathway that the tin ions traveled during the depletion of the tin area at the corner of the finish termination, closest to the dendrite.

Testing at 0.5 V resulted in the formation of copper deposits along the tips of cathode electrodes, as shown in Figure III.19. The copper dendrites grew mostly during the first 30 minutes of testing, and then increased relatively slowly, but still continued to grow after 4 hrs. The process of dendrite growth correlates with the darkening of the copper base layer at the termination, which indicates the anodic dissolution and corrosion of copper in areas across the dendrites. Neither tin deposits nor corrosion of the tin finish at the anode terminal were observed.

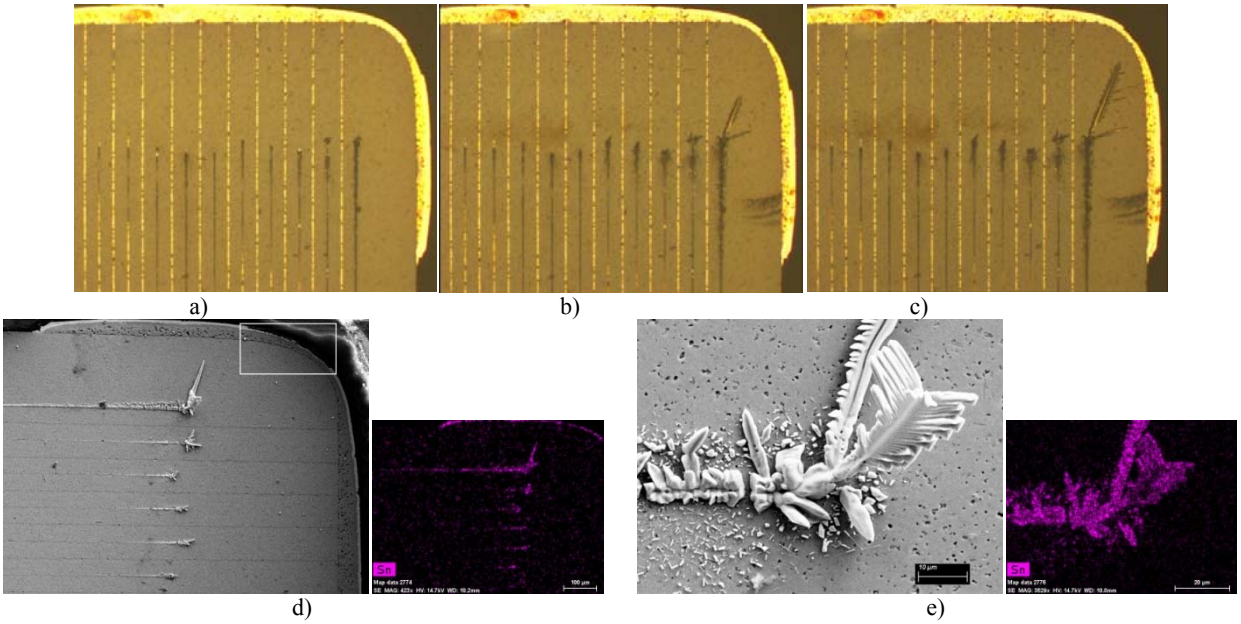

Figure III.18. Formation of tin dendrites in a 0.47 µF 50 V BME capacitor from Mfr. A after 30 min (a), 90 min (b), and 120 min (c) of WLT at 0.8 V. Figures (d) and (e) show tin deposits and dendrites after the part failed via short circuit. A square outline in figure (d) indicates an area of the tin anodic dissolution (corrosion). Note that the long tin dendrite bent and broke during SEM examinations.

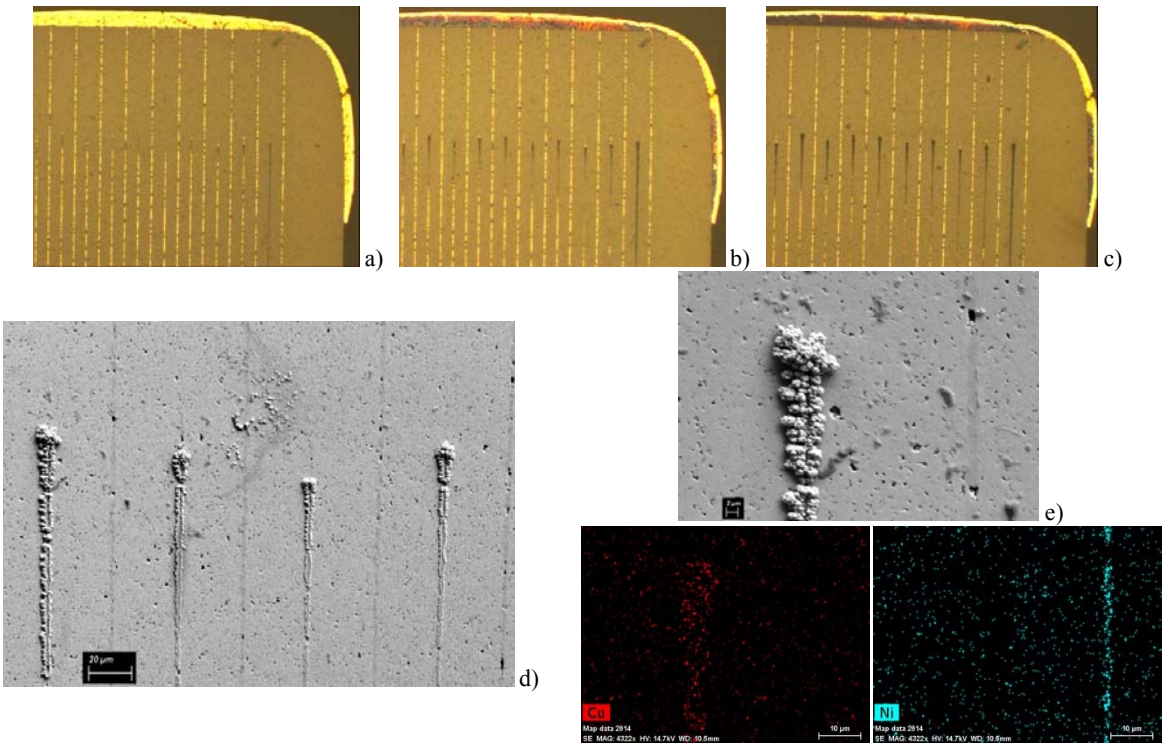

Figure III.19. Formation of copper dendrites in a 0.47 µF 50 V BME capacitor from Mfr. A after 1 min (a), 35 min (b), and 4 hrs (c) of WLT at 0.5 V. Note the darkening of the copper base terminal metallization across the cathode tips. Figure (d) shows an overall SEM view, and figure (e) is a close-up SEM/EDS image of a copper dendrite.

IV. Results of HSSLV testing

Typical variations of leakage current in cross-sectioned PME and BME capacitors during HSSLV testing are shown in Figure IV.1, and indicate no failures in the BME parts, whereas all PME capacitors failed by the end of the testing. Both part types had the same size, value of capacitance and rated voltage, and similar thickness of the dielectric (~1 mil). Therefore, the difference in their behavior can be attributed to the differences in the metallization system used. Some noise in the leakage current below ~ 2×10^{-8} A was due to the sensitivity of the used meter. The maximum level of the current after a short circuit, ~ 1.5×10^{-5} A, was due to the 100 kOhm limiting resistors connected in series with each capacitor.

Additional testing of 1825 0.47 µF 50 V capacitors from four vendors (20 BME and 20 PME total) showed no failures in BME parts, whereas 17 out of 20 PME parts failed the testing. Resistances of the parts measured after testing were in the MOhm range for the BME capacitors and in the Ohm and kOhm range for the PME capacitors.

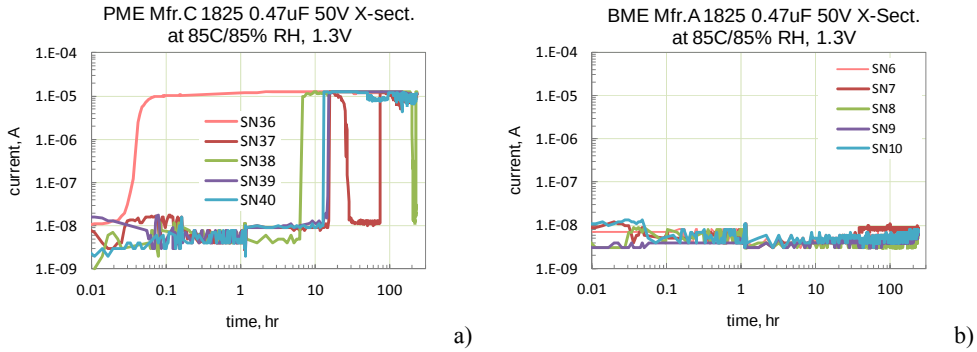

Figure IV.1. Variation of leakage currents in five 1825 0.47 µF 50V PME (a) and five 1825 0.47 µF 50V BME (b) capacitors during humidity low-voltage testing at 85°C/85 %RH 1.3V.

Silver dendrite growth from the cathodes to the anodes was observed on most failed PME capacitors. Examples of these dendrites are shown in Figure IV.2. In both pictures, the depletion of the anode electrodes indicates the source of the silver ions that formed dendrites. EDS analysis revealed the presence of palladium in the composition of the dendrites. Figure IV.2.b. also shows that some silver-containing precipitates were formed around the anode electrodes.

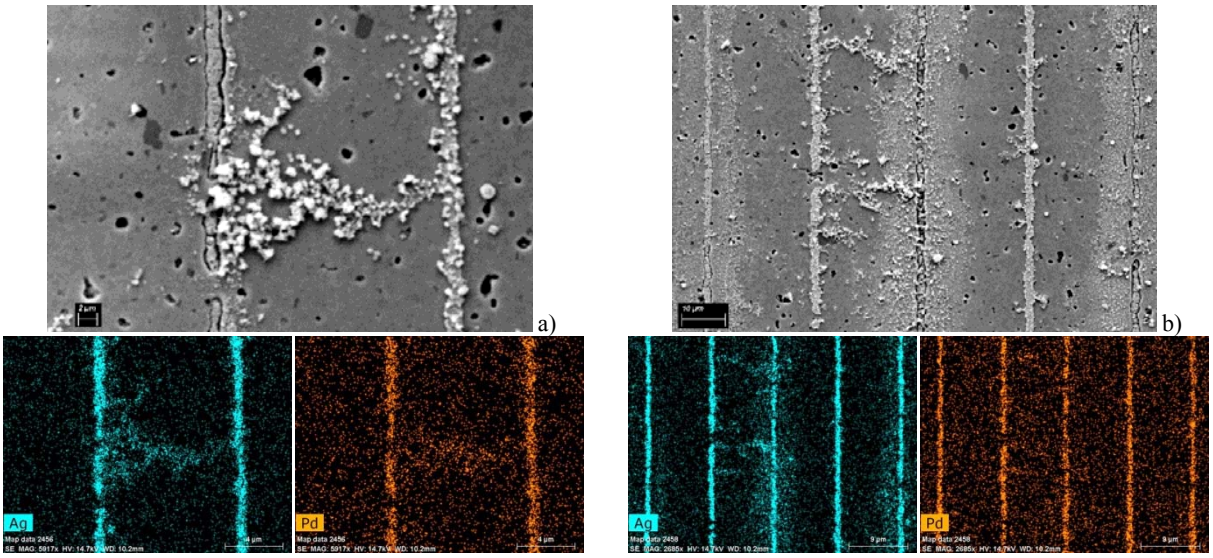

Figure IV.2. Silver dendrites in 0.47 μF 50 V PME capacitors caused failures after HSSLV testing. The anode electrode is on the left of fig.(a) and in the center of fig.(b).

Figure IV.3 shows more examples of silver dendrites detected on failed 0.47 μF 50 V PME capacitors. In all cases, normal dendrite growth from cathode to anode was observed. However, in some cases (see Figure IV.3.b) substantial silver deposits were observed at the anode electrodes as well. The presence of tin (see Figure IV.3.b) and lead (see Figure IV.4.) deposits along the silver cathodes was detected by EDS mapping.

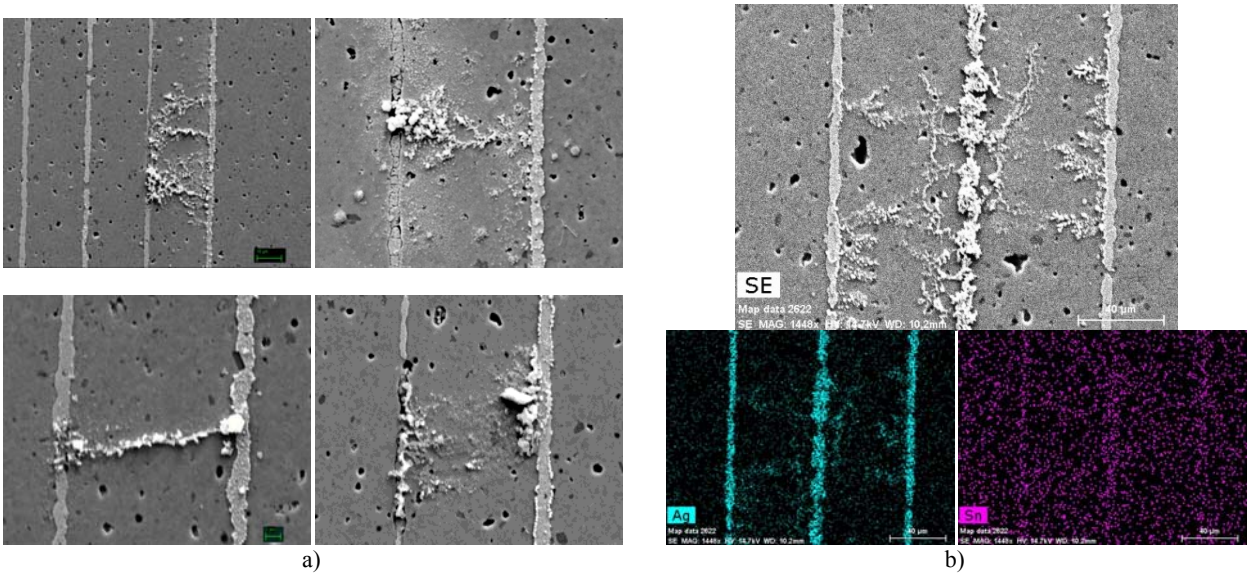

a) b)

Figure IV.3. Examples of silver dendrites (a) growing from cathode electrodes (right) to anode electrodes (left). Note the silver depletion at the anode areas. Figure (b) shows similar Ag dendrites growing from cathode electrodes (edge electrodes) toward the central anode electrode. Note the silver and tin deposits at and around the anode.

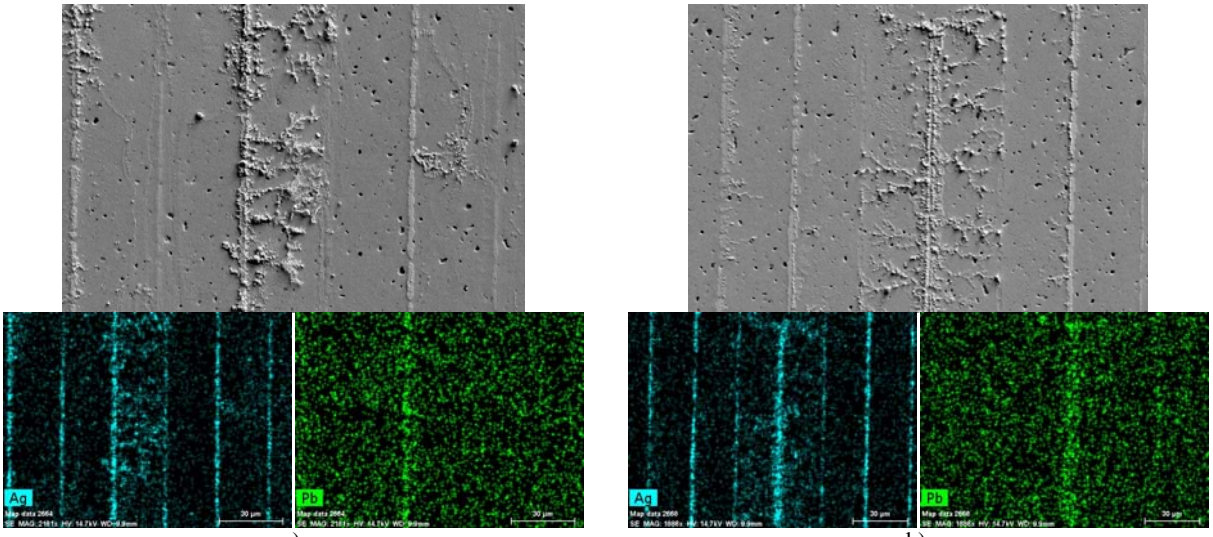

a) b)

Figure IV.4. Silver dendrites and lead deposits along the cathode electrodes in PME capacitors caused failures during HSSLV testing.

Lead was detected not only in areas of silver dendrite formation, as shown in Figure IV.5.a, but also along the cathode electrodes close to the cathode termination, as shown in Figure IV.5.b.

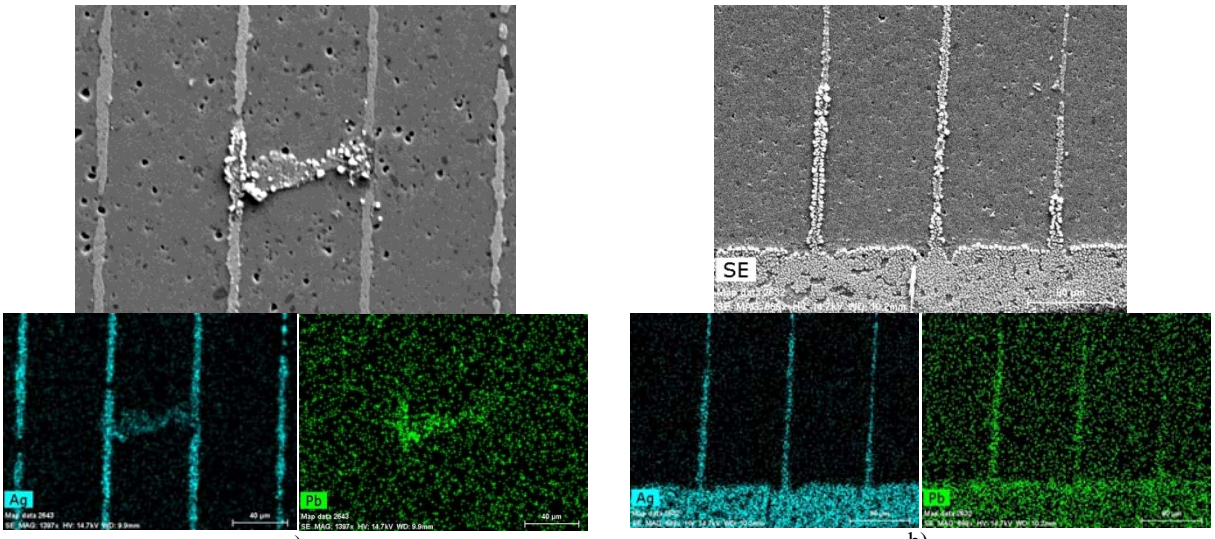

a) b)

Figure IV.5. Silver and lead in the dendrite composition (a) causing failure during HSSLV testing and lead deposits at the base of the cathode electrodes in PME capacitors (b).

Although BME capacitors did not fail electrically, SEM/EDS analysis revealed evidence of electrochemical migration of nickel, tin, copper, and lead. Figure IV.6 shows tin-, and nickel-containing deposits on the surface of an 1825 0.47 µF 50 V capacitor from Mfr. C. Tin was found to have formed a halo around the anode electrode tips that had developed amorphous, globular, Ni-containing deposits. EDS mapping of the deposits at the anode electrode tips revealed the presence of oxygen and carbon (see Figure IV.7) suggesting the formation of nickel oxides and carbonates.

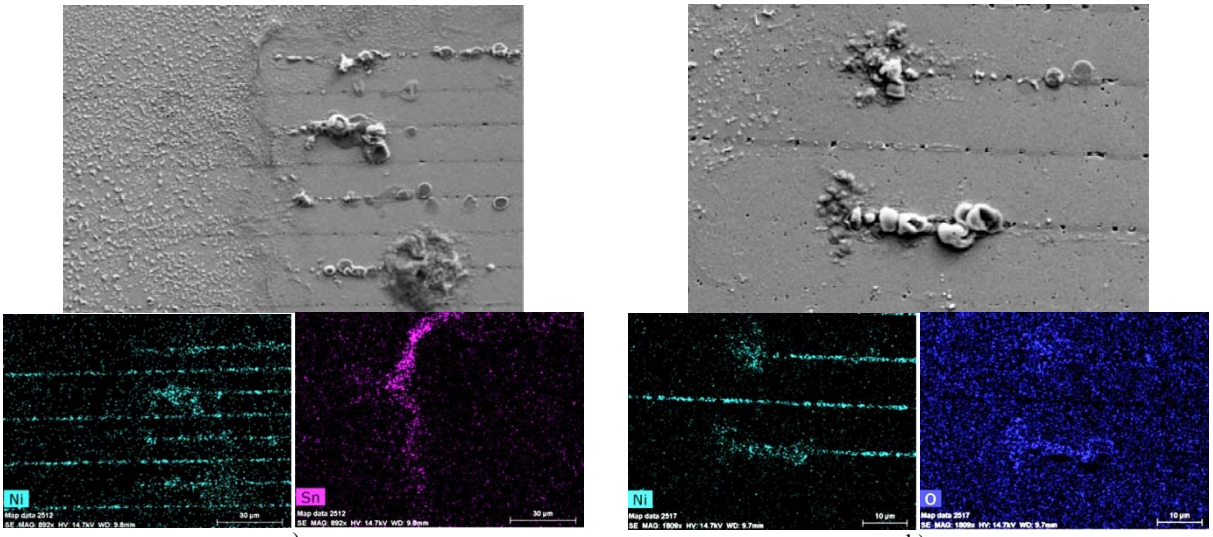

a) b)

Figure IV.6. SEM and EDS mapping images of the cathode terminal areas of 1825 0.47 µF 50 V BME capacitors from Mfr. C after HSSLV testing showing amorphous, nickel-containing deposits at the tips of anode electrodes.

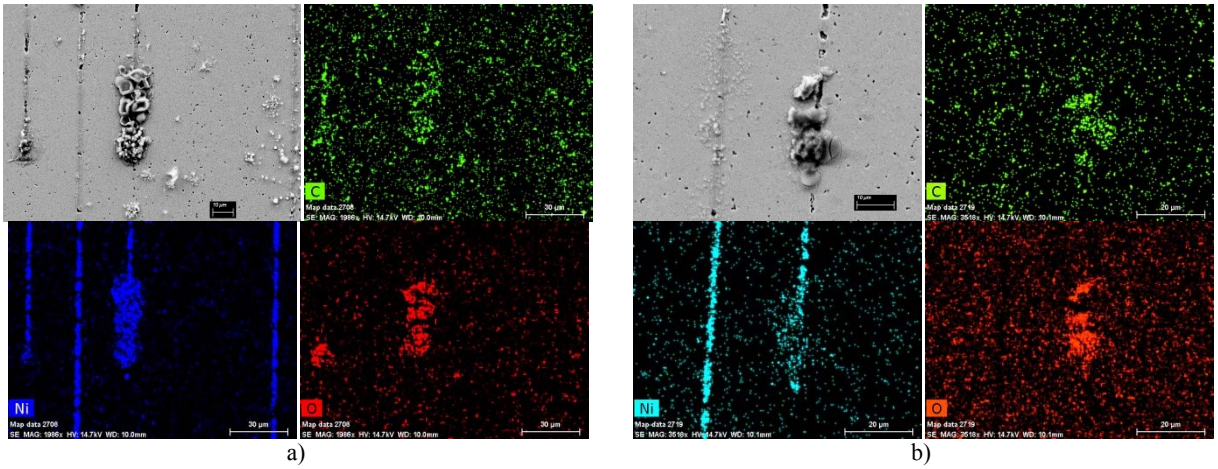

a) b)

Figure IV.7. Examples of nickel oxide and nickel carbonate formations at the anode electrode tips of 1825 0.47 µF 50 V capacitors from Mfr. A after HSSLV testing.

Copper and nickel deposits on the surface of 1812 BME 1 µF 50 V capacitors from Mfr. C after 44 hrs of HSSLV testing had carbon and oxygen in their compositions (see Figure IV.8), thus confirming the formation of nickel and copper carbonates. Copper/carbon compositions formed amorphous structures at the tips of the anode electrodes (see Figure IV.8.a); however, the presence of copper deposits was also detected along the cathode electrodes (Figure IV.8.b). Note that in SEM, the nickel carbonate stripe along the central anode electrode (see Figure IV.8.a) appears as a bright white area. This is due to charging and indicates that nickel oxide/carbonate composition is a good insulator.

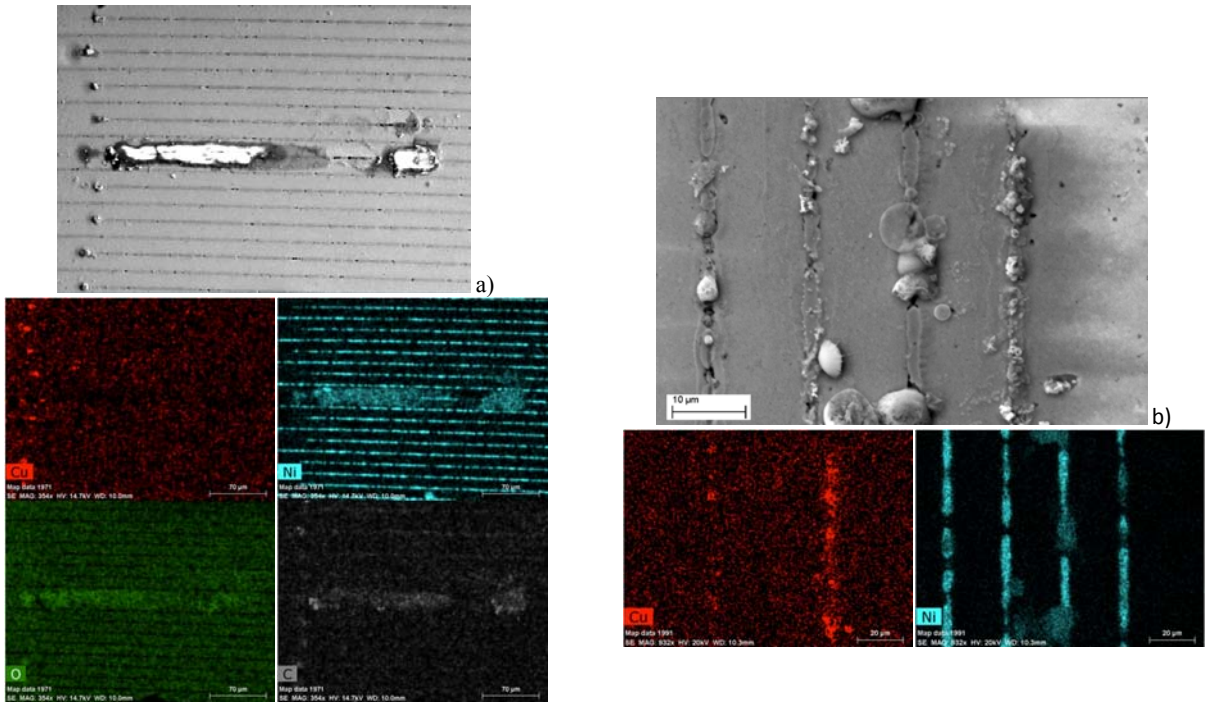

Figure IV.8. SEM and EDS images of the surface of BME 1 µF 50 V capacitors from Mfr. C after 44 hrs of HSSLV testing at 1.3 V 85°C/85 % RH. Note the copper formations at the tips of the anode electrodes in figure (a) and along the cathode electrodes in figure (b). Nickel compositions were formed along the anode electrodes.

Copper and lead dendrites were also revealed in other samples of 1 µF 50 V capacitors as shown in Figures IV.9 and IV.10. These dendrites originated from cathode electrodes and grew toward anodes. In all cases, these dendrites were observed at the edge areas close to the anode terminals of the part.

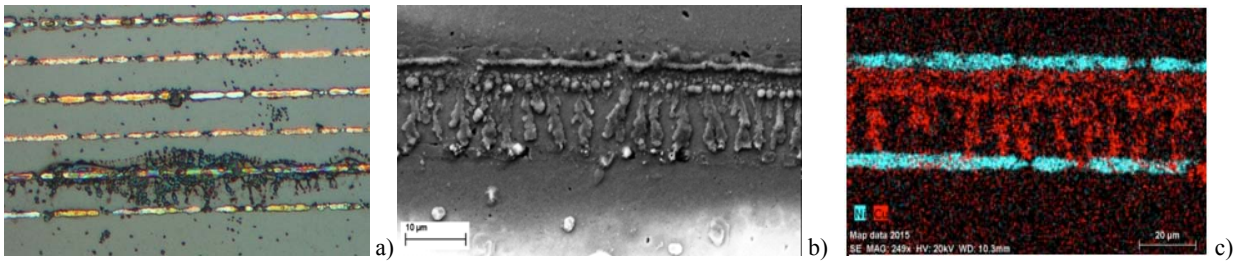

Figure IV.9. Overall optical (a) view, close-up SEM image (b), and EDS mapping of edge cathode in a 1 µF 50 V BME capacitor showing growth of copper dendrites.

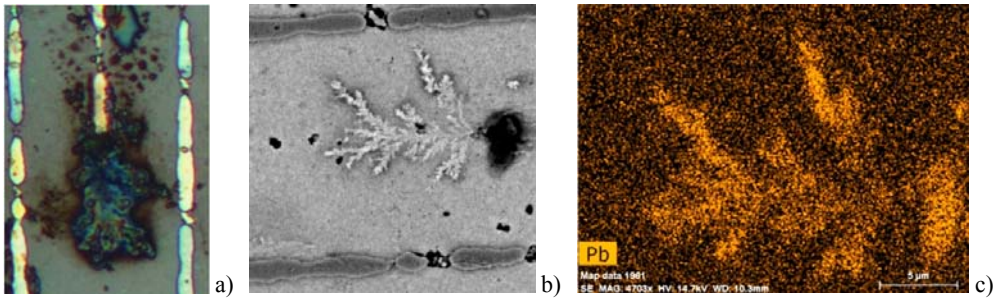

Figure IV.10. Optical (a), SEM (b), and EDS (c) images of a lead dendrite formation at the tip of a cathode electrode in a 1 µF 50 V BME capacitor. Note that this part was soldered using Sn/Pb eutectic solder alloy.

V. Discussion

Contrary to our initial expectations that ECM in cross-sectioned capacitors is limited to the metals used in internal electrodes of the capacitors (Ag/Pd for PME and Ni for BME), experiments show that all metals, including those used in the termination metallization system, and even metals used in the solder, play an important role in the dendrite growth and failures of MLCCs.

Failures during WLT in both BME and PME capacitors were mostly due to Pb and Sn dendrites that shorted edge cathode electrodes to the anode terminations. Copper dendrites were observed at the edge electrodes and at the tips of cathode electrodes in BME capacitors. The source of Sn is the termination finish, whereas the lead was dissolved from the Pb/Sn solder alloy used to attach wires to the parts or Sn/Pb finish (see Table 1). Copper was extracted from the base metallization layer in the termination. In all cases, pitting corrosion was observed either on the termination finish, solder alloy, or copper base metallization.

Several studies of electrochemical processes on the surface of PWBs with different solder alloys showed that the lead-rich alloys are much more vulnerable to corrosion and are more susceptible to ECM compared to tin-rich alloys [17-20]. Takemoto at.al. [17] found that the main constituent of dendrites during ECM of Pb/Sn alloys was lead, and the threshold voltage for ECM initiation in pure water is ~ 0.7 V, while tin dendrites in pure tin specimens were formed starting from 5 V only. Our results show that the susceptibility of Sn/Pb alloys to ECM is greater than for silver and copper, which is in agreement with the results of Takemoto at.al. [17]. However, in ceramic capacitors, both, Pb and Sn can form dendrites at voltages as low as 0.5 V.

Standard electrochemical potentials for Pb and Sn are close (~ -0.13 V). However, due to the passivation of tin by a thin, ~2 nm, SnO layer, the corrosion rate of Pb is about two orders of magnitude higher than that measured for Sn [21]. Lead readily dissolves in water forming Pb2+ ions that migrate and form dendrites at the cathode much faster than tin, which is consistent with our results. At some conditions, Pb+ ions form precipitations on the surface that by reaction with water and gaseous contaminants (CO_2) form compositions of lead oxide, PbO, lead hydroxide, $Pb(OH)_2$, and carbonates ($PbCO_3 \bullet 2Pb(OH)_2$). In our experiments, these precipitations formed halo layers around tips of cathode electrodes.

Most studies of ECM and dendrite growth for metals used in PWBs (Pb, Sn, and Cu) were carried out using WDTs at relatively large voltages, typically 2 V and greater. For example, IPC-TM-650 describes a standard test to assess the propensity of materials used for PWB design for surface electrochemical migration and requires testing at 10 V. Our data show that Pb and Sn dendrites in MLCCs can be formed within a few minutes at 1.3 V, and within hours at voltages as low as 0.5 V. Tree-like copper dendrites, with large branches, were formed at the tips of cathode electrodes in BME capacitors at 1.3 V. Also, some copper deposits, which indicated the beginning of dendrite growth, were observed after 17 hours of testing at voltages as low as 0.25 V. Considering that a longer time period of formation can lead to a higher probability of "dendrite poisoning" [13], it is possible that at voltages below ~ 0.5 V the dendrites might not grow large enough to cause a short circuit failure.

Results of WLT showed that lead and tin dendrites had different morphologies: in the parts soldered with eutectic Sn/Pb alloys, Pb dendrites had a needle-like structure, and Sn dendrites were fern-like. For the parts with only a minimal amount of solder, some tin dendrites were formed at the edges of copper- and lead dendrites. Halo-like formations of deposits on the surface of the anode termination end margin had two layers, with Pb-containing precipitates located closer to the tips of the cathode electrodes than the Sn-containing precipitates. This corresponds to the results of Lee et.al. [20] who observed dendrite-shaped filaments of the Pb-rich phase on the cathode and globular filaments for the Sn-rich phase that formed before reaching the cathode. Also, in cases where the eutectic Sn/Pb solder was minimal, and the finish layer on the capacitor was pure Sn, it was observed that the pure Sn dendrite formations were long and narrow. This is contrary to the fuller fern-like formations found in capacitors with exposed Sn/Pb alloy.

Due to the easiness of Pb dissolution, Pb dendrites and precipitates are formed first, while Sn begins to dissolve later, forming dendrites and precipitates further from the cathode. A two-layered structure of the corrosion products for Sn/Pb solder, with Sn-rich phases at the outer layer and looser Pb-rich phases at the inner layer, was also observed in [22]. Noh and Fung [18] observed formation of Sn and Pb dendrites on the surface of PWBs during WDT at voltages from 6.5 V to 15 V. Similar to our results, the structure of the Sn-rich dendrites can be described as fern-like.

Additional experiments showed that the dissolution and diffusion of Pb+ ions from Sn/Pb eutectic solder can occur in unbiased cross-sectioned capacitors at WLT conditions after a few hours of exposure to deionized water. Figure VI.1 shows corrosion of solder that was obviously due to a galvanic effect in cells consisting of Sn-rich and Pb-rich phases. The Pb-rich phases manifest evidence of anodic dissolution of Pb. Oxidation and carbonization of the dissolved Pb ions result in formation of Pb/O/C composition of corrosion products at the Pb-rich areas. Also, formation of Pb-containing thin (~100 nm) platelets was observed on the surface of ceramics, some distance from the termination. Considering that the composition of these platelets included oxygen and carbon, their formation can be explained by the diffusion of dissolved Pb+ ions reacting with hydroxyl ions OH^- in the water and CO_2 from the air, which likely resulted in hydrocerussite crystalline platelets, $Pb_3(OH)_2(CO_3)_2$. Similar platelets on the surface of 63Sn-37Pb solder joints were observed in [23] after ~ 20 mins of exposure to deionized water at room temperature.

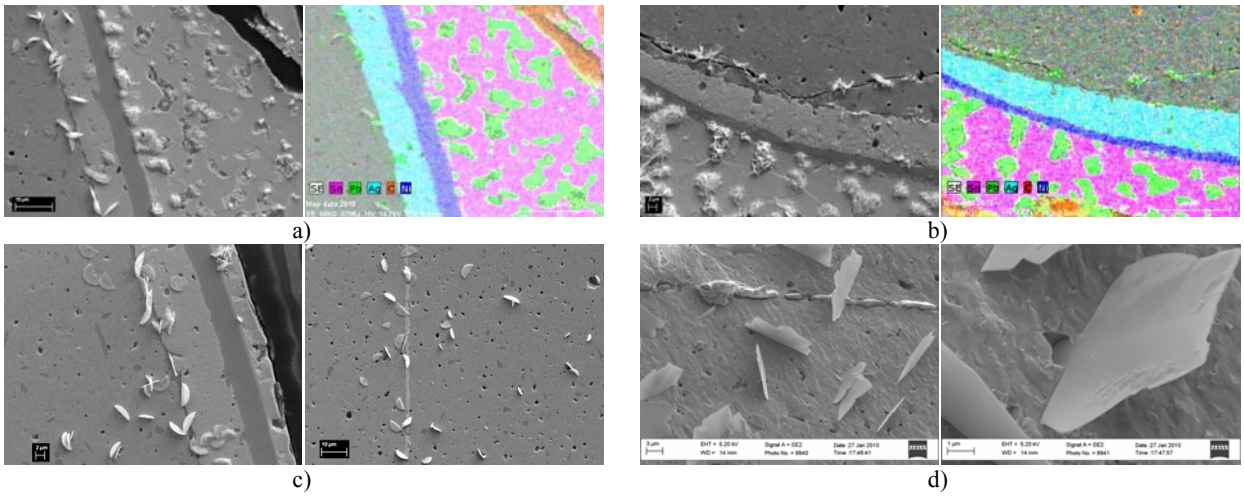

Figure VI.1. Corrosion of eutectic Sn/Pb solder on cross-sectioned PME 0.1μF, 100V, 1825, capacitors from Mfr. A after unbiased WDT at 12 μm water layer thickness for 4 hours (a, b). Figures (c) and (d) show more examples of the platelets formed on the surface of cross-sectioned (c) and fractured (d) capacitors. Note that Pb, O, and C were detected in the composition of the platelets indicating a hydrocerussite-like structure.

Although silver is considered the metal most susceptible to migration, no Ag dendrites were formed in PME capacitors during WLT. The fact that dendrites did not grow between the electrodes might be partially attributed to a high passivity of the Ag/Pd alloy used for the internal electrodes. However, the termination has a large volume of pure silver (base electrode) that could produce plenty of dissolved Ag+ ions to form dendrites at the tips of the cathode electrodes. Most likely, this does not happen because of the presence of tin finish or tin/lead solder. Anodic indexes, AI, which indicate the compatibility of different metals [24], are -0.15 V for Ag, -0.65 V for Sn, and -0.7 V for Pb. The difference between AI_Ag and AI_Sn or Sn/Pb is more than 0.5 V, which means that these metals are not compatible and would cause galvanic corrosion even in controlled environments. In the couple Sn-Ag or Sn/Pb-Ag, Ag will serve as a cathode, and thus the dissolution of Ag in humid environments will be suppressed (cathodic corrosion protection). For nickel, AI = -0.3 V and the difference between AI of the base and finish metals for BME capacitors (~0.3 V) is much less than for PME capacitors. For this reason, generally BME capacitors should be less susceptible to electrochemical degradation and failures in the presence of moisture.

It is known that ECM intensifies as the distance between electrodes decreases [18]; however, our results show that this distance is not the major factor controlling the growth of dendrites. After anodic extraction/dissolution from the termination or solder, the Sn and Pb ions are travelling a long distance, ~ 100 to 300 μm, compared to the distance between internal electrodes, ~ 20 μm, before deposition at the closest edge cathode electrode. Considering that the diffusion coefficient of metal ions in water, D, is in the range from 5×10^{-10} to 9×10^{-10} m^2/s, the diffusion length after time t is $L = d^2/t$. At t = 1 minute L is in the range from 200 μm to 300 μm. This means that the ions dissolved from the termination metallization can easily reach areas of internal electrodes to start dendrite formation, and the rate of anodic dissolution is the most important factor in the process of dendrite growth.

Large, 5 μm to 10 μm in size, tetragonal crystals of hydrated stannic oxide, SnO_2, were formed on the surface of the solder at the terminals, most likely due to a galvanic cell reaction between Sn-rich and Pb-rich phases of solder [23]. Micrometer- and sub-micrometer size tetragonal SnO_2, and probably PbO_2, crystals were also observed on the

surface of anode margin areas, at some distance from the anode terminal. These crystals were likely formed when tin and lead ions dissolved from the solder were diffusing toward the cathode electrodes and interacting with hydroxide anions, OH^-, in the alkaline area of the water layer near the cathode [1]. This interaction results in the formation of hydroxides, $Me(OH)_2$ or $Me(OH)_4$, where Me is Sn or Pb, that precipitates on the surface and can dehydrate to form more stable MeOx crystals on the surface.

A new pattern of dendrite formations was observed during WLT of PME capacitors at 0.8 V (see Figure III.11). These dendrites grew not from the cathode electrodes, as described by the classic model of dendrite growth [16], but from the layer of deposits located between the anode and cathode electrodes. This layer was formed by Sn and Pb oxide and hydroxide precipitates. Considering that the hydrated lead oxide [25] is conductive, and some forms of tin oxide have low resistivity [26], they are likely forming a virtual cathode, from which Sn and/or Pb dendrites are growing.

Formation of dendrites that bridge the electrodes and their subsequent rupture after a short circuit might explain intermittent behavior of low-voltage failures in MLCCs with cracks. When electrodes are bridged by a tiny dendrite, this rupture might clear the short, after which the process repeats at the same or another place on the surface of the crack. However, when a relatively large dendrite is formed, the micro explosion associated with the short might create more severe damage to the structure, resulting in melting of the ceramic and a catastrophic failure (see an example in Figure V.2.). It is also possible that during such an event, the melted metal will be forced to fill out other areas of the crack, creating a permanent short.

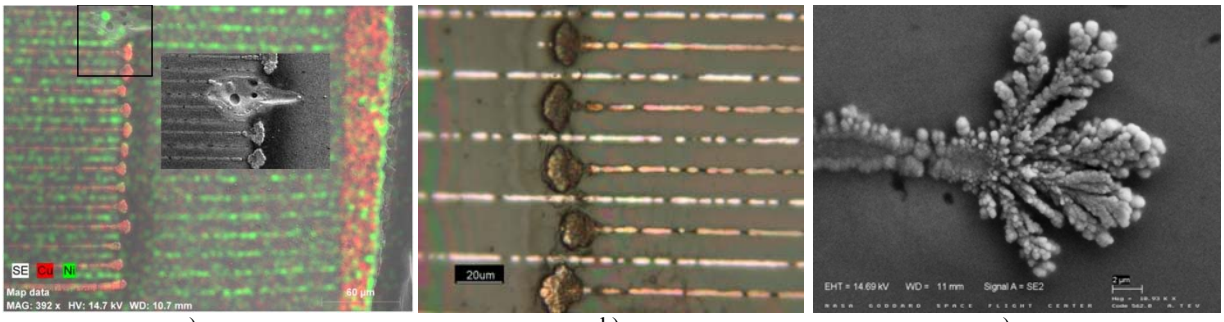

a) b) c)

Figure V.2. An example of a catastrophic failure caused by copper dendrite growth in an 1812 1 µF 50 V capacitor. These dendrites grew after 5 min at 3V, 95% RH, RT, but the failure occurred when a rated voltage was applied after the testing. Figure (a) is an overall SEM image overlapped with EDS mapping and an insert showing an area of a blown dendrite and damaged structure of the ceramic. Figure (b) is an optical and (c) is a SEM view of the copper dendrites formed at the tips of the cathode electrodes.

No silver dendrites were observed during WLT; nevertheless, their formation was the major cause of failures in PME capacitors tested during HSSLV testing at 85°C/85% RH, 1.3 V. This is likely due to the fact that anodic dissolution, diffusion, and migration of Pb and Sn ions in water occurs much faster than the dissolution of silver in the Ag/Pd alloy used in internal electrodes. A relatively fast shorting of capacitors by Sn/Pb dendrites does not allow enough time for depassivation of the palladium oxide layer that is likely the major protection against the development of Ag dendrites [8-9]. EDS analysis of most silver dendrites showed the presence of Pd in their composition, thus indicating that the major source of Ag+ is positively biased Ag/Pd electrodes. Silver depletion of anode electrodes at the site of dendrite growth provides additional evidence that the migration is not caused by dissolution of the silver base termination, but originates from the internal electrodes. It is important to note that Sn and Pb were also present in the composition of dendrites, so ECM of solder still does occur during HSSLV testing of PME capacitors.

Under WLT conditions, galvanic corrosion of finish metals (Sn, Pb) generates a substantial amount of ions that reach the cathode electrodes within a few minutes, resulting in the fast growth of dendrites. Under HSSLV test conditions, only a few (from 2 to 6) monolayers of water are absorbed. This significantly slows the anodic dissolution and diffusion processes. For PME capacitors, formation of silver and/or Ag/Pd dendrites between the adjacent electrodes became possible, and HSSLV failures are due to short circuit or intermittent contact, typically after hours of testing.

Silver precipitates located close to the anode areas were likely formed by a colloidal silver oxide [6, 27]. Considering that AgO has relatively high conductivity, from 10^3 S/cm to 10^5 S/cm [28], these formations can cause parametric failures of capacitors even without formation of shorts by silver dendrites.

None of the BME capacitors failed due to a short circuit or exhibited intermittent contacts during HSSLV testing. However, formation of copper and Pb dendrites and deposits were observed. Due to slow ECM processes, these dendrites could react with contaminations and their growth was most likely "stopped by poisoning" [13]. For these reasons, the dendrites did not grow large enough to short the capacitor or to significantly compromise the insulation resistance. Lead and copper dendrites started growing from the cathode electrodes near the anode termination, which had large concentrations of ions dissolved from the termination metallization. However, Ni-containing amorphous deposits were formed at the anode internal electrodes, in some cases far from the terminations.

According to Harsani [16], eluted Ni^{2+} ions in alkaline environments at the cathode areas might be reduced, forming complex cations ($HNiO_2^-$) that will move back to the anode:
$Ni^{2+} + 2H_2O \rightarrow HNiO_2^- + 3H^+$
At the anode, the following reaction can result in the formation of nickel oxide deposits:
$3\ HNO_2^- + H^+ \rightarrow Ni_3O_4 + 2H_2O + 2e^-$
Nickel oxide can also react with CO_2 from the air, forming carbonates ($NiCO_3$), which explains the presence of carbon in the anode deposits.

It is also possible that nickel hydroxide, $Ni(OH)_2$, reacts with CO_2, forming complex ions [29]:
$Ni\text{-}OH + CO_2 \rightarrow NiOCO_2^- + H^+$
These ions would also migrate to the anode, forming $NiCO_3$ carbonates. Both types of precipitates have a tendency to agglomerate, forming amorphous deposits at the anode electrodes. Due to the high resistivity of nickel oxide [30], these formations do not substantially affect the resistance of capacitors or cause electrical failures.

In a simplified form, the processes of (a) ECM on the surface of BME and PME capacitors that result in dendrite growth at the cathode electrodes, (b) the formation of precipitates between electrodes, and (c) the formation of deposits on anode electrodes, are shown in Figure V.3. As discussed before, depending on materials and test conditions, the precipitates might be conductive (typical for PME capacitors) or isolative (typical for BME capacitors). Obviously, a more significant degradation of electrical characteristics of the parts is expected in the first case.

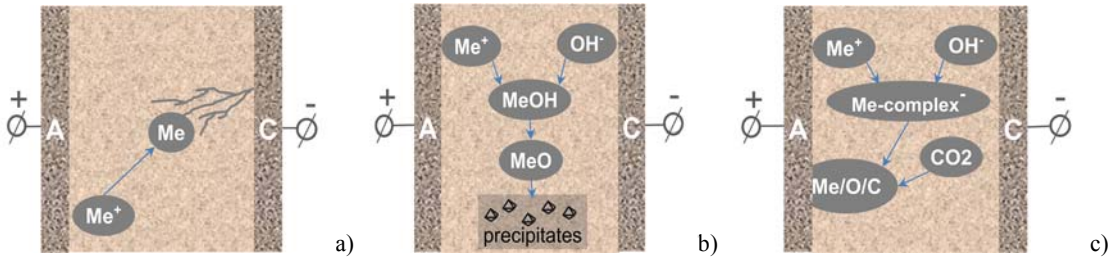

Figure V.3. Simplified schematic of electrochemical processes in MLCCs: cathode dendrite growth (a), formation of precipitations (b), formation of anode deposits (c).

VI. Conclusion

1. Short circuit failures, due to the dendrite growth on the surface of cross-sectioned ceramic capacitors, were observed at voltages in the range from 0.5 V to 1.3 V, during water layer testing for both PME and BME capacitors, and at 1.3 V during HSSLV testing at 85°C, 85% RH, for PME capacitors only.

2. Under the water layer test conditions, metals that are the most susceptible to dendrite growth are Pb > Sn, for PME capacitors, and Pb > Sn ≥ Cu, for BME capacitors. Pb, Sn, and Cu ions contributing to dendrite growth were generated by anodic dissolution of the termination finish and solder. These dendrites grew mostly at the edge cathode electrodes on the surface of the anode end margin area. Some Pb and Sn dendrites were growing not from the cathode electrodes, but from the Pb and/or Sn-containing conductive deposits that had formed 10 µm to 20 µm from the edge cathode electrodes. Pb, Sn, and Cu dendrites were the prevailing reason for short circuit failures during WLT, but deposits of these metals were also observed during HSSLV testing.

3. No silver dendrites in PME capacitors or nickel dendrites in BME capacitors were detected during WLT. However, most HSSLV test failures of PME capacitors were due to the formation of shorting Ag or Ag/Pd dendrites

growing from cathode electrodes. Conductive colloidal deposits of silver were observed close to the anode areas of the internal electrodes.

4. HSSLV testing resulted in failures of 17 out of 20 PME capacitors, however, none of the 20 tested BME capacitors failed. Nickel-containing amorphous deposits (combination of nickel oxide and carbonates) formed at the anode internal electrodes, and in some cases, filled the area between the anode and cathode electrodes. These deposits had a high resistance and did not cause severe degradation of the electrical characteristics of the part.

5. The differentiating feature of ECM and dendrite growth in MLCCs is the presence of different metals that form galvanic cells, which enhance substantially the anodic elution of metal ions, such as Pb, Sn, and Cu, at low voltages. Results and analysis show that PME capacitors, due to the presence of Sn/Pb – Ag galvanic cells, are more susceptible to Pb and Sn dendrite growth, compared to BME capacitors, which have Sn/Pb – (Ni or Cu) cells, that have more compatible anodic indexes. Nickel does not form dendrites at low voltages, but creates Ni/O/C deposits that have a relatively high resistance and, consequently, does not cause short circuit failures in BME capacitors.

6. Due to the ease of electromigration of termination and eutectic Sn/Pb solder metals, typically used for hi-rel parts, cracks that extend through the terminals, rather than the body, are the most dangerous and are much more likely to cause catastrophic or intermittent failures in MLCCs.

7. HSSLV testing at 1.3 V can detect failures in PME capacitors with electrodes exposed to environments, but it is not effective for revealing defective BME capacitors. New, more effective test conditions are being evaluated.

VII. Acknowledgment

The NASA Electronic Parts and Packaging (NEPP) Program and the Office of the Chief Technologist, through NASA's Space Technology Research Fellowship program, sponsored this work. The author is thankful to the Program Manager Michael Sampson, GSFC, for support of this work.

VIII. References

[1] D. Minzari, M. S. Jellesen, P. Moller, and R. Ambat, "On the electrochemical migration mechanism of tin in electronics," *Corrosion Science,* vol. 53, pp. 3366-3379, 2011.

[2] R. Chittick, E. Gray, J. Alexander, M. Drake, and E. Bush, "Nondestructive Screening for Low Voltage Failure in Multilayer Ceramic Capacitors," *Components, Hybrids, and Manufacturing Technology, IEEE Transactions on,* vol. 6, pp. 510-516, 1983.

[3] H. C. Ling and A. M. Jackson, "Correlation of silver migration with temperature-humidity-bias (THB) failures in multilayer ceramic capacitors," *IEEE Transactions on Components, Hybrids, and Manufacturing Technology,* vol. 12, pp. 130 - 137, 1989.

[4] K. Wakino, T. Murata, and Y. Sakabe, "Failure analysis and screening method for low voltage problem on monolithic ceramic capacitor," MURATA MANUFACTURING CO., LTD. 1982. Available:

[5] B. I. Noh, J. B. Lee, and S. B. Jung, "Effect of surface finish material on printed circuit board for electrochemical migration," *Microelectronics Reliability,* vol. 48, pp. 652-656, Apr 2008.

[6] J. J. Steppan, J. A. Roth, L. C. Hall, D. A. Jeannotte, and S. P. Carbone, "A review of corrosion failure mechanisms during accelerated tests - electrolytic metal migration," *Journal of the Electrochemical Society,* vol. 134, pp. 175-190, Jan 1987.

[7] M. J. Ditz and I. N. T. Asm, "*Determination of the moisture threshold for silver migration*", 1994.

[8] J. C. Lin and J. Y. Chan, "On the resistance of silver migration in Ag-Pd conductive thick films under humid environment and applied d.c. field," *Materials Chemistry and Physics,* vol. 43, pp. 256-265, 1996.

[9] N. J. Donnelly and C. A. Randall, "Refined Model of Electromigration of Ag/Pd Electrodes in Multilayer PZT Ceramics Under Extreme Humidity," *Journal of the American Ceramic Society,* vol. 92, pp. 405-410, Feb 2009.

[10] S. A. Yang and A. Christou, "Failure model for silver electrochemical migration," *Ieee Transactions on Device and Materials Reliability,* vol. 7, pp. 188-196, Mar 2007.

[11] M. Sampson, J. Brusse, and A. Teverovsky, "Humidity Steady State Low Voltage Testing of MLCCs (Based on NESC Technical Assessment Report)," in *CARTS USA*, Jacksonville, Fl, 2011.

[12] A. DerMarderosian, "THE ELECTROCHEMICAL MIGRATION OF METALS," in *Proc. Int. Society of Hybrid Microelectronics*, 1978, pp. 134-141.

[13] G. DiGiacomo, "*Reliability of Electronic Packages and Semiconductor Devices* ": McGrow Hill, 1996.

[14] B. I. Noh, J. W. Yoon, W. S. Hong, and S. B. Jung, "Evaluation of Electrochemical Migration on Flexible Printed Circuit Boards with Different Surface Finishes," *Journal of Electronic Materials,* vol. 38, pp. 902-907, Jun 2009.

[15] D. Y. Zheng, J. Swingler, and P. Weaver, "Current leakage and transients in ferroelectric ceramics under high humidity conditions," *Sensors and Actuators a-Physical,* vol. 158, pp. 106-111, Mar 2010.

[16] G. Harsanyi, "Electrochemical processes resulting in migrated short failures in microcircuits," *Components, Packaging, and Manufacturing Technology, Part A, IEEE Transactions on,* vol. 18, pp. 602-610, 1995.

[17] T. Takemoto, R. M. Latanision, T. W. Eagar, and A. Matsunawa, "Electrochemical migration tests of solder alloys in pure water," *Corrosion Science,* vol. 39, pp. 1415-1430, Aug 1997.
[18] B. I. Noh and S. B. Fung, "Behaviour of electrochemical migration with solder alloys on printed circuit boards (PCBs)," *Circuit World,* vol. 34, pp. 8-13, 2008.
[19] J.-Y. Jung, S.-B. Lee, H.-Y. Lee, Y.-C. Joo, and Y.-B. Park, "Electrochemical Migration Characteristics of Eutectic Sn-Pb Solder Alloy in NaCl and Na2SO4 Solutions," *Journal of Electronic Materials,* vol. 38, pp. 691-699, 2009.
[20] S.-B. Lee, H.-Y. Lee, M.-S. Jung, Y.-B. Park, and Y.-C. Joo, "Effect of the composition of Sn-Pb alloys on the microstructure of filaments and the electrochemical migration characteristics," *Metals and Materials International,* vol. 17, pp. 617-621, 2011.
[21] V. Brusic, D. D. Dimilia, and R. Macinnes, "Corrosion of lead, tin, and their alloys," *Corrosion,* vol. 47, pp. 509-518, Jul 1991.
[22] D. Li, P. Conway, and C. Liu, "Corrosion characterization of tin–lead and lead free solders in 3.5 wt.% NaCl solution," *Corrosion Science,* vol. 50, pp. 995-1004, 2008.
[23] H. Chang, H. Chen, M. Li, L. Wang, and Y. Fu, "Generation of Tin(II) Oxide Crystals on Lead-Free Solder Joints in Deionized Water," *Journal of Electronic Materials,* vol. 38, pp. 2170-2178, 2009.
[24] J. Qiu, "Corrosion in Microelectronics, ASM Handbook," in *Corrosion: Environments and Industries*. vol. 13C, S. D. Cramer and B. S. Covino, Eds., ed: ASM International, 2006, pp. 613-622.
[25] R. C. Keezer, D. L. Bowman, and J. H. Becker, "Electrical and Optical Properties of Lead Oxide Single Crystals," *Journal of Applied Physics,* vol. 39, pp. 2062-2066, 1968.
[26] M. Batzill and U. Diebold, "The surface and materials science of tin oxide," *Progress in Surface Science,* vol. 79, pp. 47-154, 2005.
[27] S. J. Krumbein, "METALLIC ELECTROMIGRATION PHENOMENA," *Ieee Transactions on Components Hybrids and Manufacturing Technology,* vol. 11, pp. 5-15, Mar 1988.
[28] U. Kumar Barik, S. Srinivasan, C. L. Nagendra, and A. Subrahmanyam, "Electrical and optical properties of reactive DC magnetron sputtered silver oxide thin films: role of oxygen," *Thin Solid Films,* vol. 429, pp. 129-134, 2003.
[29] C.-H. Lee and C.-H. Lee, "A study on nickel hydroxide crystallization characteristics," *Korean Journal of Chemical Engineering,* vol. 22, pp. 712-716, 2005/09/01 2005.
[30] P. S. Patil and L. D. Kadam, "Preparation and characterization of spray pyrolyzed nickel oxide (NiO) thin films," *Applied Surface Science,* vol. 199, pp. 211-221, 2002.